Lab 5: X-ray Diffractometer

Otho Ulrich, Mike Pirkola, Jacob Burke, Andrew Messecar

April 18, 2017

Abstract

Western Michigan University's new X-ray Diffractometer is used to probe four samples. The absorption depths are reported for each sample. Bragg diffraction is discussed as it pertains to a cubic geometry. The diffraction pattern from a sodium-chloride (NaCl) sample is analyzed in detail. The lattice contant is computed for this sample. For three amorphous, organic samples – wood, grease, and plastic – the average distance between atoms is computed, and from this the density is computed. The lattice constant computed for NaCl agrees strongly with known values, and the median compute density across all amorphous samples deviates from carbon density by approximately 10%.

1 Introduction

Bragg diffraction of X-rays is a useful method for characterising the atomic and molecular structure of materials. Many mechanical and electric properties are functions of the atomic structures that constitute materials. Bragg diffraction uses the wave theory of electromagnetic radiation to predict how x-rays will interact with the atomic lattice of a crystal. The spacing between atoms can be measured by inference, and these spacings are called the lattice constants.

We attempt to compute the lattice constant from an x-ray diffractometer reading of a sample of NaCl, or common salt. NaCl forms a cubic crystal structure, so it has a single lattice constant. This will be computed from the diffraction pattern and compared to known values. Three amorphous samples will also be analyzed: plastic of an unknown type; grease; and wood. These materials are not expected to have rigid crystal structures, but the average spacing between atoms can be ascertained from the diffraction pattern. These materials are made of mostly carbon, with some hydrogen and oxygen. We therefore expect their densities to be nearly that of amorphous carbon.

2 Bragg Diffraction

The diffraction angle of x-rays by atoms in a crystal lattice or other molecule depends on the distance between atoms. The lattice constants of a crystal describe the distances and angles between atoms, but in the case of a cubic lattice such as NaCl, there is only one relevant lattice constant. Bragg diffraction predicts strong x-ray signals at diffraction angles that produce constructive interference. Figure 1 illustrates the geometry of Bragg diffraction; the distance between planes d is the lattice constant, and the Bragg condition

$$2d \sin\theta = n\lambda, \tag{1}$$

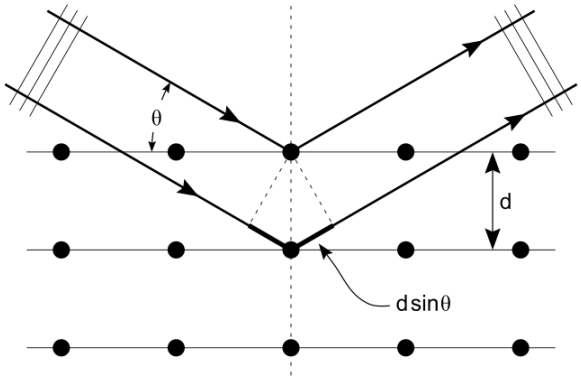

Figure 1: Bragg diffraction from a cubic crystal lattice. Plane waves incident on a crystal lattice at angle θ are partially reflected by successive parallel crystal planes of spacing d. The superposed reflected waves interfere constructively if the Bragg condition $2d\sin\theta = n\lambda$ is satisfied. [1]

where λ is the photon wavelength of the X-ray and n a positive integer describes the angles at which strong signals should be detected. [2]

The modern approach to analyzing materials by Bragg diffraction is to interpret the output as the reciprocal space representation of the lattice positions. An inverse Fourier transform then gives the positions that make the lattice. The HighScore Plus software, associated with the Empyrean XRD, is used to perform these operations. [5]

A crystal powder sample will have random orientations across all possible rotations in 3 dimensions; we call this powder diffraction. In a cubic crystal the Miller indices $(h\ k\ l)$ describe the orientation of the planes, predicting periodic lattice points along the z-axis that will produce constructive interference. While the lattice constant does not change, each orientation may result in a different diffraction spacing, so a powder diffraction will result in a diffraction pattern where signals are observed at many angles; observe Figure 2. The lattice constant can be computed in each case.

3 Material Structure

The structure of some samples tested here are known. NaCl is a face-centered cubic lattice with lattice constant $a = 564.02$pm. [9] This closely agrees with the value reported by Wallace and Barrett: $a = 5.64 \pm 0.0005$Å. [10] The allowed miller indices for a FCC lattice are given in Table 1, with the computed diffraction spacing, and some of the geometries are shown in Figure 2.

Amorphous materials consisting of mostly carbon have complex structures. Therefore, they are difficult to analyze in detail. [8] The diffraction pattern peak should reach a maximum at the angle θ corresponding to the average distance between atoms, and lesser peaks can be expected as indicators of other prominent structures within a sample. These values will be determined and a density computed from the average distance between atoms. [2]

h	k	l	Spacing ()	$2\theta(^\circ)$	Reflected Int. (%)
1	1	1	3.26	27.367	8.7
0	0	2	2.82	31.704	100
0	2	2	1.99	45.449	64.3
1	1	3	1.70	53.87	2.2
2	2	2	1.63	56.474	20.2
0	0	4	1.41	66.229	8.7
1	3	3	1.29	73.072	1
0	2	4	1.26	75.294	22.5
2	2	4	1.15	83.994	16.2

Table 1: Allowed Miller indices (h k l) for NaCl. For each, the predicted diffraction spacing along the axis normal to the sample surface is predicted, and the incidence angle with its expected reflected intensity. [10] [5]

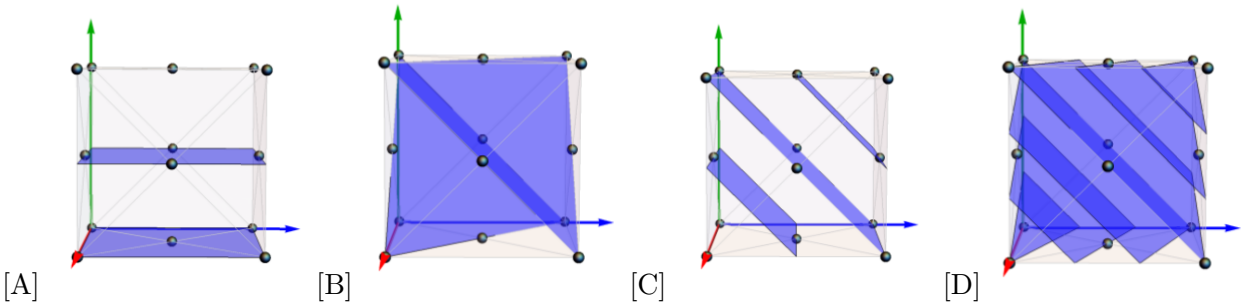

Figure 2: Four of the atomic plane orientations of a face-centered cubic lattice that result in Bragg diffraction. The Miller indices (h k l) for each structure are [A] (0 0 2) [B] (1 1 1) [C] (0 2 2) [D] (1 3 3). The predicted diffraction spacings are tabulated in Table 1

Mat.	Packing Frac.	Density (g/cm^3)	Atomic Mass (g)	MAC (cm^2/g)	Pen. Depth (μm)
NaCl	0.7	2.165	-	73.7	206
Carbon	0.6	2.0	1.99442×10^{-23}	4.3	4460

Table 2: Properties of interest for the materials analyzed in this study. Values for the amorphous materials are assumed to be those of amorphous carbon. Packing fractions are rough estimates. The mass attenuation coefficients are taken from the NIST Hubbell and Seltzer database, and used by HighScore Plus to compute the penetration depth. Densities and atomic mass are as reported on Wikipedia, April 17, 2017. [4] [9] [3]

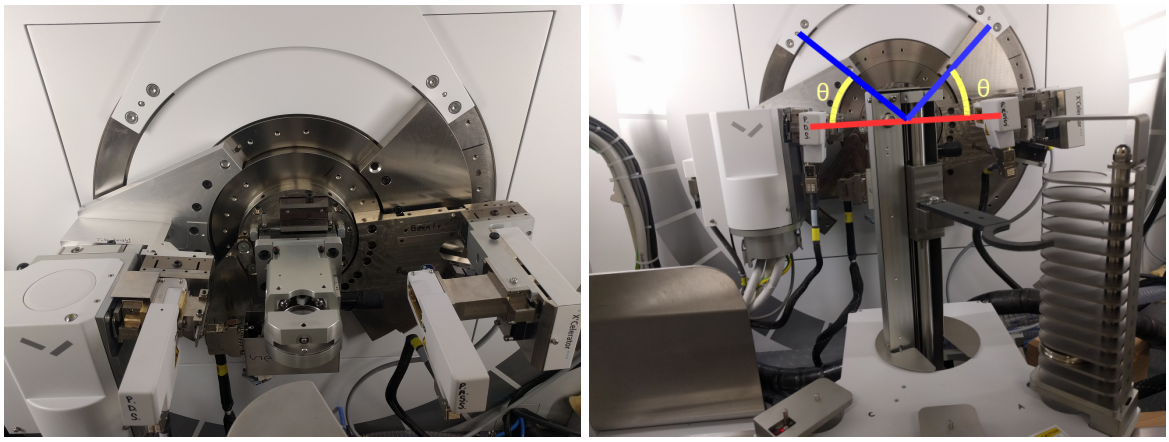

Figure 3: The PANalytical Empyrean x-ray diffractometer. A sample is placed in a bin at the center. X-rays are generated in the arm on the left, diffracted at an incidence angle θ by the sample at the center, and detected at a reflected angle θ by the X'Celerator in the arm on the right. Each scan runs through $\theta = \{5°..45°\}$.

3.1 Penetration Depth

The penetration depth of Cu K-α_1 is computed for each material. This is the depth in a material by which 98% of the photons at this energy will have attentuated. The defining formula

$$I_L = I_0 \times e^{-(\frac{\mu}{\rho}\rho L)} \tag{2}$$

is valid for symmetric (gonio) scans. [5] The HighScore Plus software computes the penetration depth from the mass attentuation coefficient, specific gravity of the material, and a powder packing fraction. These values are tabulated in Table 2 along with the computed penetration depths. Penetration depth is computed for an incidence angle 90°, which gives maximum penetration.

4 X-ray Diffractometer

An Empyrean x-ray diffractometer by PANalytical [6] was used to collect a diffraction pattern from each sample. In this machine, an x-ray source emits onto a material sample, and a detector records x-rays diffracted at the angle of incidence; see Figure 3. X-rays are created by accelerating electrons toward a copper anode (Figure 4). The X'Celerator detector is an x-ray sensor consisting of 127 single-file barrier detectors with copper K-α efficiency $> 94\%$ [7].

The sample container depth was not measured during the experiment – a major oversight. A best guess for the sample tray depth is $1.5 \pm .3$ cm. If the penetration depth of a material exceeds this distance, diffraction from the container may be observed, contaminating the results.

4.1 Computational Details

The phases of the x-rays cannot be measured, so the HighScore Plus software from PANalytical determines the phase by fitting predicted profiles. To identify the NaCl pattern, a background is determined using the minimum 2nd derivative method with "bending factor" = 5, "granularity" = 20, and using smoothed input data. Peaks are located with "minimum significant" = 10.00,

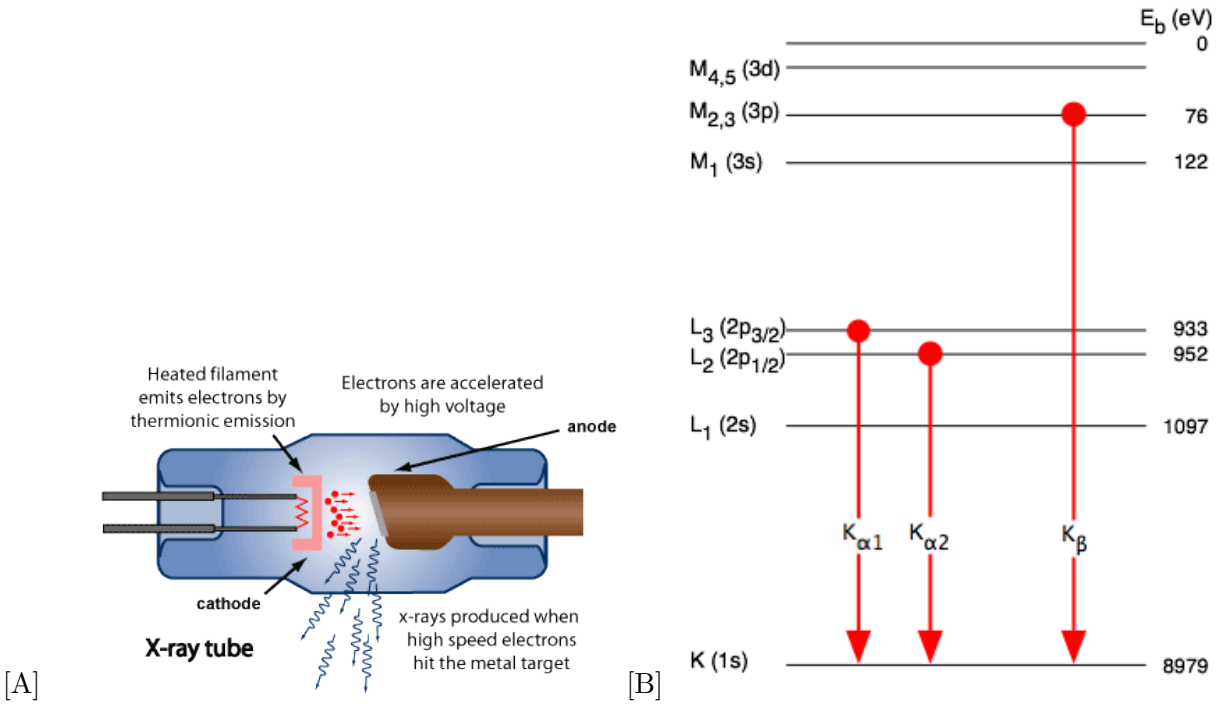

Figure 4: [A] X-rays are generated when collisions with accelerated electrons knock electrons in the copper atoms of the anode out of the K shell. When the electrons fall back to the K shell, x-rays are emitted with energies indicated in [B]. These energy values are important for predicting the x-ray diffraction pattern from Bragg diffraction. [2] [11]

Copper Emission	Energy (eV)	Frequency (Hz)	Wavelength (Å)
K-α_1	8046	1.946×10^{18}	1.541
K-α_2	8027	1.941×10^{18}	1.393
K-β	8903	2.153×10^{18}	1.545

Table 3: Copper K-α and K-β x-ray photon properties. The K-α_1 is the primary driver of x-ray diffraction in this study, but the other x-rays are also present in smaller numbers.

2θ (°)	Spacing (Å)	Refl. Int. (%)	h	k	l	Lattice Const. (Å)
27.369 (0.000)	3.2588 (0.000)	2.32 (0.73)	1	1	1	5.64±0.35
31.638 (0.002)	2.8258 (0.002)	100 (0.00)	0	0	2	5.65±0.40
45.385 (0.001)	1.9967 (0.004)	16.75 (0.74)	0	2	2	5.65±0.56
53.873 (0.000)	1.7004 (0.000)	0.58 (0.74)	1	1	3	5.64±0.66
56.430 (0.000)	1.6293 (0.000)	4.36 (0.78)	2	2	2	5.64±0.69
66.180 (0.000)	1.4109 (0.000)	8.96 (0.03)	0	0	4	5.64±0.80
75.291 (0.000)	1.2612 (0.000)	5.54 (0.75)	0	2	4	5.64±0.89
83.949 (0.000)	1.1518 (0.002)	2.42 (0.85)	2	2	4	5.64±0.98

Table 4: Observed peaks from the NaCl sample. Diffraction spacings and the reflected intensity ratios are computed for each. The Miller indices are determined by matching angular position with Table 1. In parentheses is the ratio difference from predicted values in that table. These values are best matches reported by the HighScore software, but uncertainties were not reported. An inspection by eye gives approximately ±0.05° for 98% confidence in the observed angle 2θ, and the computed standard error for the diffraction spacing is ±0.20Å.

"minimum tip width" = 0.01, "maximum tip width" = 1.00, and "peak base width" = 2.00. [5].

The lattice constant a is computed by

$$a = \text{diffraction spacing} \times \sqrt{h^2 + k^2 + l^2}. \tag{3}$$

For the amorphous samples, peaks are identified by hand to within a standard error of ±0.05°. We use the copper K-α wavelength from table 3: $\lambda = 1.541 \times 10^{-10}$Å. The spacing is calculated as

$$d/n = \lambda / (2 \sin \theta) \tag{4}$$

with n = 1. Using the atomic mass and packing fraction from Table 2 allows the density ρ to be computed as

$$\rho = \frac{\text{atomic mass}}{\text{unit cell volume} \times \text{packing fraction}} \tag{5}$$

where the unit cell is assumed to be face-centered cubic with side length equal to the computed average distance.

5 Results

The penetration depths of NaCl and amorphous carbon are 206 μm and 4,460 μm, respectively. 98% of all photons will have attentuated at this depth in the material.

The observed diffraction pattern from NaCl is presented in Figure 5. The HighScore software was able to identify the copper Bragg diffraction pattern, which was prominent by inspection. Table 4 contains the values obtained by the program, with divergence from predicted values. The lattice constant for NaCl's face-centered cubic structure is computed from each value, all returning approximately 5.64, with relative error between 7% and 18%.

Several peaks were identified for each amorphous sample. In each case, a spacing was determined and a density computed. These are reported in Table 5. The densities ran from 0.087 to 4.359 g/cm^3, which is a run of about 1.5 orders of magnitude. The median value is 2.22 g/cm^3.

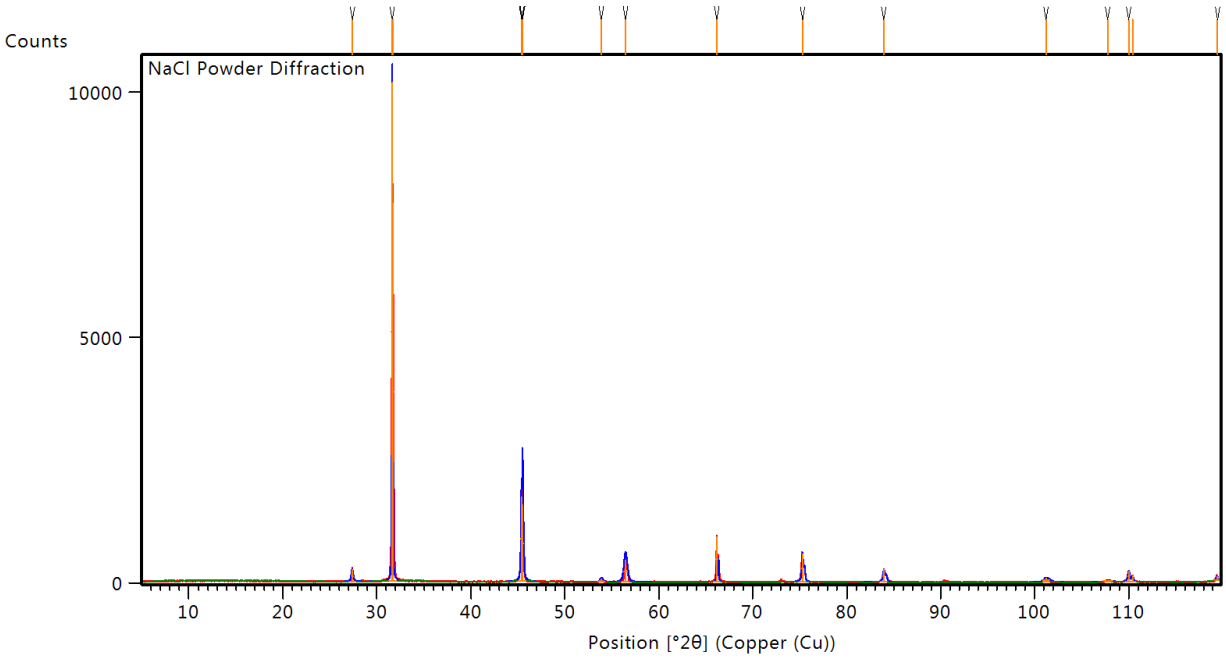

[A]

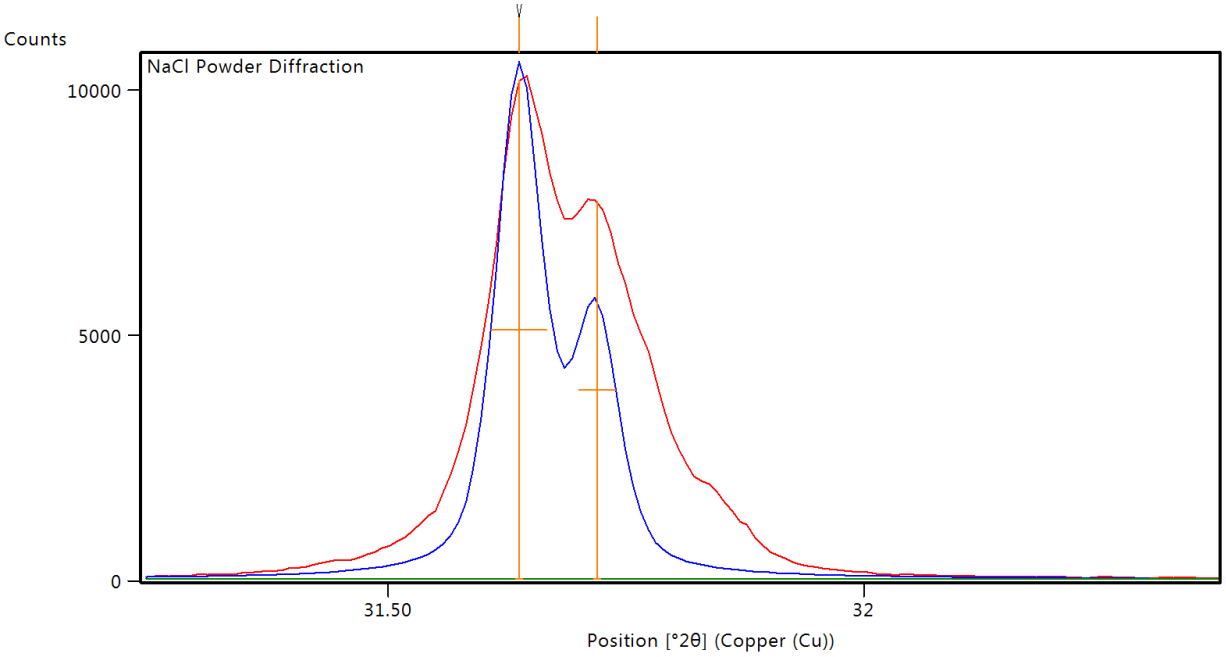

[B]

Figure 5: [A] HighScore Plus identified the characteristic NaCl diffraction pattern from Cu K-α emission, and this is used to fit the phase and in turn determine the lattice constant. [B] At the most prominent peak, the detector measurements (red) strongly correlate with the computed diffraction lines (blue).

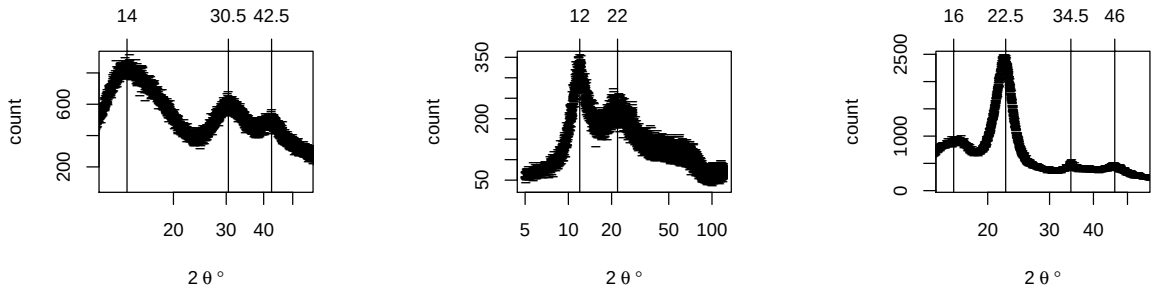

[A] [B] [C]

Figure 6: Diffraction curves observed from the three amorphous samples, presented on log scales: [A] unknown plastic; [B] grease; [C] wood. The largest peak should correspond to the average distance between atoms. Secondary peaks may indicate a secondary structure. An interpretation is attempted in Section 6.

Sample	$2\theta \pm 0.5$ (°)	Spacing (Å)	Density (g/cm^3)	Ratio (2g/cm^3)
Plastic*	14.0	6.32 ± 0.45	0.136 ± 0.029	0.07 ± 0.02
Plastic	30.5	2.93 ± 0.09	0.549 ± 0.038	0.27 ± 0.04
Plastic	42.5	2.13 ± 0.05	3.451 ± 0.243	1.73 ± 0.24
Grease*	12.0	7.37 ± 0.62	0.087 ± 0.021	0.04 ± 0.02
Grease	20.0	4.44 ± 0.22	0.385 ± 0.057	0.19 ± 0.06
Wood	16.0	5.54 ± 0.35	0.200 ± 0.038	0.10 ± 0.04
Wood*	22.5	3.95 ± 0.17	0.545 ± 0.070	0.20 ± 0.07
Wood	34.5	2.60 ± 0.07	1.899 ± 0.153	0.95 ± 0.15
Wood	46.0	1.97 ± 0.04	4.359 ± 0.265	2.18 ± 0.27

Table 5: Observed peaks in diffraction pattern in amorphous samples. * indicates greatest peak, likely the peak associated with the average spacing between atoms. The ratio relative to the known carbon density 2.0 g/cm^3 is also tabulated.

6 Conclusion

The penetration depths fall short of the 1.2 cm limit imposed by the sample container tray depth, so we do not expect that there are significant signals observed from the sample container over these collections. Signals observed may therefore reliably be considered emergent from Bragg diffraction by the samples.

The diffraction pattern of NaCl was easily and clearly identified by the HighScore Plus program. The angles of incidence and reflection deviate from predictions only in the fourth order of precision or less, as do the diffraction spacings. The reflection intensities, however, deviate by a large amount from predictions: many showing approximately $\frac{1}{4}$ the predicted intensity. It's suspicious that each of these errors falls within a small range around $\frac{1}{4}$, and this may indicate a computational error rather than an experimental one.

The lattice constant for NaCl was computed in each case, and all agree to within 3 orders of precision with the known lattice constant 5.64 Å. This method of measuring the lattice constant appears to be very reliable.

The amorphous samples present several peaks from which to compute an average diffraction spacing. Only one of the computed densities falls precisely around the density of amorphous carbon (wood, 46.0°). Considering a cubic structure using the average distance is a rudimentary approach, and the fact that computed densities are all within 1.5 orders of magnitude of carbon's density is remarkable. It should also be noted that the median value across all of these densities is 2.22 g/cm^3, which only differs from carbon by about 10%. It may be reasonable to consider that each of these peaks indicates a prominent component to the structure, so taking them all into account provides a better estimation of the density.

References

[1] *Bragg diffraction 2*. URL: https://commons.wikimedia.org/wiki/File:Bragg_diffraction_2.svg.

[2] Clem Burns. *X-ray Diffraction*. Lab Guide. Western Michigan University, Mar. 2017.

[3] *Carbon*. Apr. 2017. URL: https://en.wikipedia.org/wiki/Carbon.

[4] J.H. Hubbell and S.M. Seltzer. *Tables of X-Ray Mass Attenuation Coefficients and Mass Energy-Absorption Coefficients from 1 KeV to 20 MeV for Elements Z=1 to 92 and 48 Additional substances of Dosimetric Interest*. 1996. URL: http://www.nist.gov/pml/data/xraycoef/index.cfm.

[5] PANalytical. *HighScore Plus Version 4.5*. www.panalytical.com/Xray-diffraction-software/HighScore/Specifications.htm. 2016.

[6] *PANalytical - Empyrean*. Apr. 2017. URL: http://www.panalytical.com/Empyrean.htm.

[7] *PANalytical - X'Celerator*. Apr. 2017. URL: http://www.panalytical.com/XCelerator/Specifications.htm.

[8] Sarah L. Price. "Predicting crystal structures of organic compounds". In: *Chem. Soc. Rev.* 43 (7 2014), pp. 2098–2111. DOI: 10.1039/C3CS60279F. URL: http://dx.doi.org/10.1039/C3CS60279F.

[9] *Sodium Chloride*. Apr. 2017. URL: https://en.wikipedia.org/wiki/Sodium_chloride.

[10] W.E. Wallace and W.T. Barrett. "Studies of NaCl-KCl Solid solutions." In: *Journal of the American Chemical Society* 76 (1954), pp. 366–369. DOI: 10.1021/ja01631a014.

[11] *X-ray Tube*. URL: http://www.arpansa.gov.au/images/basics/xraytube.png.